JMEPEG (2018) 27:3932–3939
https://doi.org/10.1007/s11665-018-3486-4

1059-9495/$19.00

Cryorolling-Induced Texture, Mechanical Properties and Fracture Behavior of Al-Mg-Si Alloys During Cold Deformation

Xianwei Ren, Yuanchun Huang, and Yu Liu

(Submitted October 1, 2017; in revised form May 13, 2018; published online July 3, 2018)

This study investigated the texture, mechanical properties, and fracture behavior during cold working of cryorolled (CR) Al-Mg-Si alloys. An x-ray texture goniometer was used to examine the crystallographic texture, and tensile tests were performed to understand the deformation behavior in more detail. SEM/EBSD/TEM was used to observe the microstructures and fracture morphology of the alloy during cryorolling. The microstructures indicated that a large number of ultrafine grains and dislocations formed after cryorolled. The recrystallization was prohibited due to low temperature during deformation. The ultrafine grains and dislocation strength improved the tensile strength from 279.38 MPa for the room-rolled alloy to 313.98 MPa for the cryorolled alloy; better plasticity (4.6%) was observed in the CR sheet. Ductile and intergranular fractures were observed in the CR sheet deformation from 20 to 90%.

Keywords Al-Mg-Si alloy, cryorolled, fracture behavior, mechanical properties, texture

1. Introduction

Heat-treatable Al-Mg-Si alloys are widely used in the automobile industry because of their excellent comprehensive properties (Ref 1-4). With stricter regulations imposed on automobile industry, achieving the desired strength and plasticity of the consistent materials has become increasingly important (Ref 5). However, conventional processing methods cannot meet these requirements. A few studies have been performed on the mechanism underlying the simultaneous improvement in strength and plasticity. Ultrafine grains (UFG) play a key role (Ref 6-9). Ultrafine grains (UFGs) play a key role. UFG crystals are prepared using various methods, but current research has primarily focused on mechanical alloying, gas-phase condensation of particulates and consolidation, electro-deposition, and severe plastic deformation (SPD). In this study, UFGs of Al-Mg-Si alloy sheets were studied after cryorolling, wherein a sheet was rolled at cryogenic temperature.

Recently, many researchers have given considerable attention to cryorolled (CR) alloys of the 6xxx series. Yadollahpour et al. (Ref 10) and Sushanta et al. (Ref 11) studied the mechanical properties of CR Al-Mg-Si alloy sheets and found that cryorolling deformation simultaneously improved the sheet strength and ductility of the aged ultrafine-grained alloy. Yu et al. (Ref 12, 13) studied how grain size and precipitation affected the strength and ductility of 6061 alloy sheets through asymmetric cryorolling. Nageswara rao et al. (Ref 14) investigated the effect of post-cryorolling treatment on the microstructural and mechanical behavior of ultrafine-grained Al-Mg-Si alloys. Huang et al. (Ref 15, 16) investigated the microstructural and mechanical properties of age-hardened CR AA6061 alloy. They are all agreed with the theory of UFG strengthening (Ref 17).

However, there have been only a few studies regarding severe plastic deformation at cryogenic (liquid nitrogen) temperatures and its effect on the microstructures of Al-Mg-Si alloys before heat treatment. In particular, the texture, mechanical properties, and fracture behavior of CR Al-Mg-Si alloys (20-90% rolling) have not been widely investigated. It is important to understand the differences between cryorolling and conventional rolling during deformation. According to Niranjani et al. (Ref 18), no secondary phases were observed in the XRD patterns after cryorolling and conventional rolling. Murayama (Ref 19) and Venkateswarlu (Ref 20) also found that the secondary phases dissolve after large plastic deformation (ECAP and severe extrusion). Hence, the effect of secondary phases was ignored in this study. In many previous studies, cryorolling was shown to improve the alloy strength through impeded dynamic recovery and facilitate higher dislocation density at low temperatures during rolling.

This study was performed to understand in detail the cryorolling mechanism during 20-90% rolling in Al-Mg-Si alloys. The effect of cryorolling and conventional rolling on the texture, mechanical properties, and fracture behavior of the alloy was investigated for four reductions (20, 60, 80, and 90%). The UFG structure was observed in the CR sheet. The recrystallization texture and deformation grains were found in the sheet subjects to conventional rolling. These factors are essential for the performance and fracture behavior of CR and conventionally rolled (room temperature rolled, RTR) sheets.

2. Experimental

The exact chemical composition of the investigated Al-Mg-Si alloy is given in Table 1. The ingot was homogenized, cut

Xianwei Ren and **Yuanchun Huang**, Research Institute of Light Alloy, Central South University, Changsha 410083, China; and State Key Laboratory of High Performance and Complex Manufacturing, Central South University, Changsha 410083, China; and **Yu Liu**, Research Institute of Light Alloy, Central South University, Changsha 410083, China. Contact e-mail: science@csu.edu.cn.

and milled, followed by hot rolling to 10 mm in a "1550" rolling mill. The sheet was rolled from 10 to 1 mm, and the reduction in each pass was controlled to about 10%. The CR sheet was soaked in liquid nitrogen for 20 min and then rolled. At the middle of each pass, the sheet was soaked in liquid nitrogen for 5 min. The RTR sheet was deformed at room temperature.

The crystallographic texture was determined through three incomplete pole figures {111}, {200}, and {220} measured by an x-ray texture goniometer. The different volume fractions of the texture components were calculated.

The crystallographic texture of the sample was analyzed by electron back-scattered diffraction (EBSD) using a Sirion 200 field emission gun scanning electron microscope (SEM) at an accelerating voltage of 20 kV. Samples for electron back-scattered diffraction (EBSD) were prepared by mechanical grinding and electropolishing. The TEM specimens were prepared by an electrolyte of 30% HNO_3 in methanol.

The tensile properties of the materials were measured, and each value was obtained by averaging the results of three measurements. Tensile tests were carried out according to the international standard ISO 6892-1 (Fig. 1). The test strain-rate was 2 mm/min.

3. Results

3.1 Evaluation of Texture

The primary texture components of the Al-Mg-Si alloy are copper (C) {112} ⟨111⟩, brass (B) {011} ⟨211⟩, S {123} ⟨634⟩, goss (G) {011} ⟨100⟩ and cube (Cu) {001} ⟨100⟩ after hot rolling as shown in Fig. 2. The volume fractions of these textures are listed in Table 2. The distribution of the α-fibers and β-fibers of the RTR and CR sheets under different deformation conditions is shown in Fig. 3. In both RTR and CR sheets, goss along the α-fiber flowed to the brass orientation with increasing deformation. Goss is a metastable orientation and the fcc rolled textures adopted a typical β-fiber extending from the copper orientation through the S orientation to the brass orientation during rolling deformation (Ref 21). In this study, the volume fractions of the RTR deformation texture increased, whereas the recrystallization texture decreased before being rolled to 90% reduction. The volume fraction of the cube orientation decreased from 32.62 to 8.33% when the deformation was increased to 80%, but an inflection point appeared at 90% deformation and the cube orientation increased from 8.33 to 14.97%. For the CR sheet, the rolling textures components grew, whereas the recrystallization texture was reduced under 20-90% rolling. The recovery and recrystallization were inhibited at low temperatures during the cryorolling process. The volume fraction of the cube orientation decreased from 32.62 to 3.35% during deformation.

Furthermore, the density of the S-{123} ⟨634⟩ sharpness was high under both rolling conditions, which introduced higher stacking fault energy. Niranjani et al. found that the predominant orientation under both rolling conditions is S {123} ⟨634⟩ (Ref 18). Under 90% reduction, a portion of the S orientation was transformed to cube orientation through 40° rotation along the ⟨111⟩ axis during recrystallization in the RTR sheet. In contrast, the CR sheet preserved the high density of the metastable S orientation.

3.2 Evaluation of Properties

The mechanical properties of the RTR and CR sheets under different deformation conditions are shown in Fig. 4. The tensile strength σ_b and yield strength σ_s of the RTR and CR sheets were enhanced with increasing deformation, whereas the elongation exhibited the opposite trend. A large deformation also reduced the difference between the σ_b and σ_s values. The strength of the CR sheet increased to a greater extent than that of the RTR sheet, and the elongation was preserved at 4.03%.

3.3 Evaluation of Fracture Mechanism

The fracture morphology of the RTR and CR sheets with different deformations is shown in Fig. 5 and 6, respectively. In the RTR sheet with 20% reduction, the characteristic dimples with diameter of 10-20 μm were evenly distributed. The largest area of these dimples is shown in Fig. 5(a). Figure 5(b) shows that the dimples in the samples are unevenly distributed. Figure 5(c) shows that the major components of the fracture mechanism are ductile and intergranular fracturing. Intergranular fracturing was the major fracture mechanism when at 90% reduction, as seen in Fig. 5(d). The fracture mechanisms of the RTR sheet changed from only ductile fracture to both ductile and intergranular fracture when the reduction was increased from 20 to 90%.

The dimple features of the CR sheet with a 20% reduction were similar to the RTR sheet with a 60% reduction, but the size and diameter of the dimples were smaller than in the RTR, as shown in Fig. 6(a). Figure 6(b), (c) and (d) shows two types of fracture morphology, small dimples and tearing edges. The fracture mechanism can be classified as ductile fracture associated with intergranular fracture during cold rolling from 20 to 90%. With increasing deformation, the dimples decreased in size and the tearing edges became more prominent.

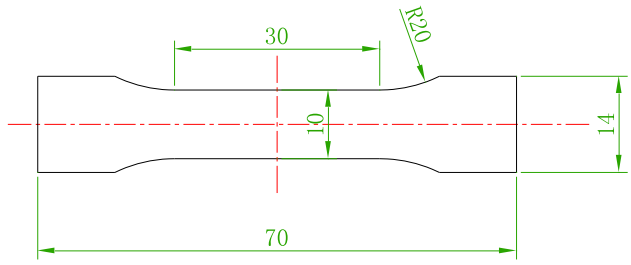

Fig. 1 Schematic diagram of the tensile specimen (unit: mm)

Table 1 Chemical compositions of Al-Mg-Si alloy (wt.%)

Alloy	Si	Fe	Cu	Mn	Mg	Cr	Ti	Al
Al-Mg-Si	0.92	0.395	0.263	0.0098	1.01	0.218	0.015	Bal.

Table 2 The volume fractions of the main texture for SR and CR sheet (%)

State	Rolling texture, %				Recrystallization texture, %			Others
	Copper	Brass	S	C + B + S	Goss	Cube	G + Cu	…
Hot-rolled	14.36	19.58	22.17	56.11	3.2	28.13	31.33	12.56
SR								
20%	7.01	21.26	24.62	52.89	13.31	23.38	39.26	10.42
60%	12.85	21.88	26.03	69.76	18.78	9.48	28.26	1.98
80%	31.59	22.20	18.49	72.28	13.14	8.33	21.47	6.25
90%	11.79	25.24	26.91	63.94	16.06	14.97	31.03	5.03
CR								
20%	14.79	17.35	22.13	54.27	14.25	24.15	38.40	7.33
60%	17.88	17.22	27.45	62.55	10.03	26.11	36.14	1.31
80%	22.54	16.80	28.42	67.76	15.06	15.46	30.52	1.72
90%	26.26	18.24	29.91	74.41	17.65	3.35	21.00	4.59

4. Discussion

4.1 Texture and Microstructure After Cryorolled

For the CR sheet with 90% reduction, the deformation texture was preserved as shown in Fig. 3(c), and (d). The matrix formed an UFG structure after large deformation, as shown in Fig. 7(a). A finer grain structure would be observed if the dynamic recovery is suppressed and the defect density is increased during cryogenic deformation (Ref 22). Many ultrafine-grained structures were distributed along the rolling direction and the size of these metastable structures was approximately 0.8-0.9 μm. EBSD characterization confirmed the texture detection results shown in Fig. 3 and 7(a). Recrystallization was effectively prevented by cryogenic deformation, as shown in Table 2.

For comparison, the grains in the RTR sheet were elongated and crushed along the rolling direction, as shown in Fig. 7(b). At 90% reduction, the volume fraction of cube orientation rebounded, as shown in Table 2. The plastic deformation heat and frictional heat may cause dynamic recovery and recrystallization during rolling to 90% reduction. Engler studied the relationship between the cube orientation and grain size and found that the large grains primarily adopt a cube orientation after recrystallization (Ref 23). However, in this research, the relationship between large grains and Cu orientation was unclear. Recrystallization occurring during the rolling process consumed the dislocations and decreased the UFG structures. This had a significant influence on the mechanical properties and fracture mechanisms, as shown in Fig. 4(a) and 5. In the CR sheet, a small cube texture intensity was observed after cryogenic deformation and a large number of ultrafine-grained structures were preserved. Thus, the ultrafine-grained structures significantly impacted the mechanical properties and fracture mechanism (Ref 24-30), as shown in Fig. 4(b) and 6.

Figure 8 shows the TEM images of the deformed samples (80, 90%) along the {100} crystal axis. For the CR sheet, the dislocation density increased from 80 to 90% rolling (Fig. 8a, c). Dislocations were scattered within the matrix, and dislocation nucleation was observed at the entanglement, as shown in Fig. 8(c). The characteristic dislocation distribution corresponded with the ultrafine structure revealed by EBSD (Fig. 7a). In the RTR sheet, the dislocations mainly accumulated at the grain boundaries and distributed along these boundaries with increasing deformation, as shown in Fig. 8(b), (d). The mechanical properties and fracture mechanism of the RTR and CR sheets differed primarily because of the low temperature effect. Lack of the heat effects in the CR sheet led to high deformation energy storage.

4.2 Cryorolled Influence on the Mechanical Properties

In the CR sheet, the defect density notably increased promoted from 80 to 90% rolling. At a low deformation temperature, the heat source had been offseted and dislocation was observed. In the RTR sheet, the dislocations showed minimal change because of the plastic deformation heat and frictional heat. These heat effects may cause dynamic recovery and recrystallization, and the dislocation was consumed during the last deformation. Thus, the effect of dislocation enhancement was nullified for the RTR sheet. CR sheet showed excellent strength and ductility after deformation.

Previous studies have shown that the grain boundaries block dislocation slips. The number of grain boundaries increased with grain refinement, thereby strongly obstructing dislocation movement. The effect of dislocation enhancement improved the strength of the sheet (Ref 5, 31). The fine grain characteristics and dislocation strengthening are shown in Fig. 7(a) and 8(a). The improved mechanical properties of the CR sheet are clearly shown in Fig. 4(b). Panigrahi et al. found that grain refinement has a more pronounced effect on the yield strength (σ_s) as compared to tensile strength (σ_b) (Ref 11). Thus, the yield strength (σ_s) closed to tensile strength (σ_b) after deformation.

The refined grains improved the strength of the material as well as its plasticity. The grain orientations on both sides of the grain boundary differed, leading to a disordered atomic arrangement in the grain boundary. The discrete distribution of atoms made the dislocation structure more complex, as shown in Fig. 8(a). The grains must cross the grain boundary to the adjacent grain during deformation, but the resistance to this movement increased because of the complicated dislocation structure, thus consuming a significant amount of energy. The plasticity of the sheet was also improved. Generally, an ultrafine structure corresponds to the proportion of large grain boundaries (Ref 18, 32). In this study, the large grain boundary content enhanced the matrix dislocation strength. The strength was improved and plasticity was maintained through the combination of fine grains and dislocation strengthening.

4.3 Cryorolled Influence on the Fracture Behavior

With increasing deformation, the dislocations gathered at the grain boundaries. Micropores formed and expanded by dislo-

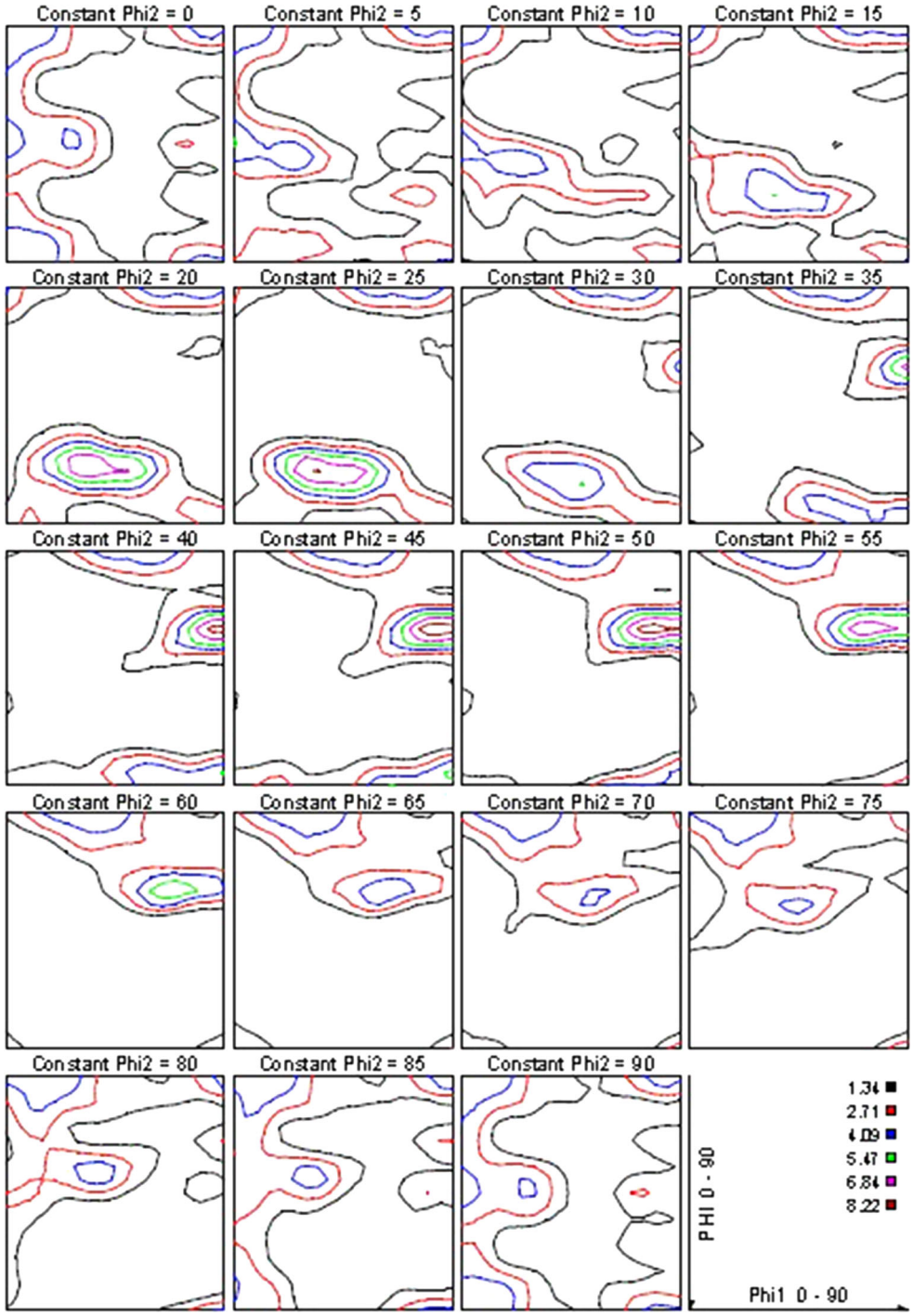

Fig. 2 The ODF with constant φ2 of AA6061 alloy hot-rolled sheet

cation aggregation when the external stress was further increased. Subsequently, a crack source was produced and small breakouts appeared at the center of the dimples, as shown in Fig. 5 and 6. Some scholars have suggested that the dislocations may accumulate in the supersaturated GP zone (Ref 5). The ductile fracture was caused by the aggregation of micropores in the GP zone. Owing to grain refinement, the dimple size continuously decreased in the CR samples.

After severe deformation, the grains were stretched and crushed, and the UFGs were widely distributed in the grain boundaries. Intergranular fracture was caused by tiny grains and the fine grains on the fracture surface coincided with the grain boundary formed during rolling. When ductile fracture extended near these grains, the crack immediately spread along the tiny grains. Finally, tear marks formed on the surface of the fracture and the different orientations between the broken grains and the substrate led to poor bonding forces with the substrate, resulting in intergranular fracture.

The sizes of the grains were approximately 1 μm in the RTR sheet, whereas for the CR sheet, a large number of ultrafine-grained structures formed. The degree of intergranular fracture intensified upon grain refinement from 20 to 90%

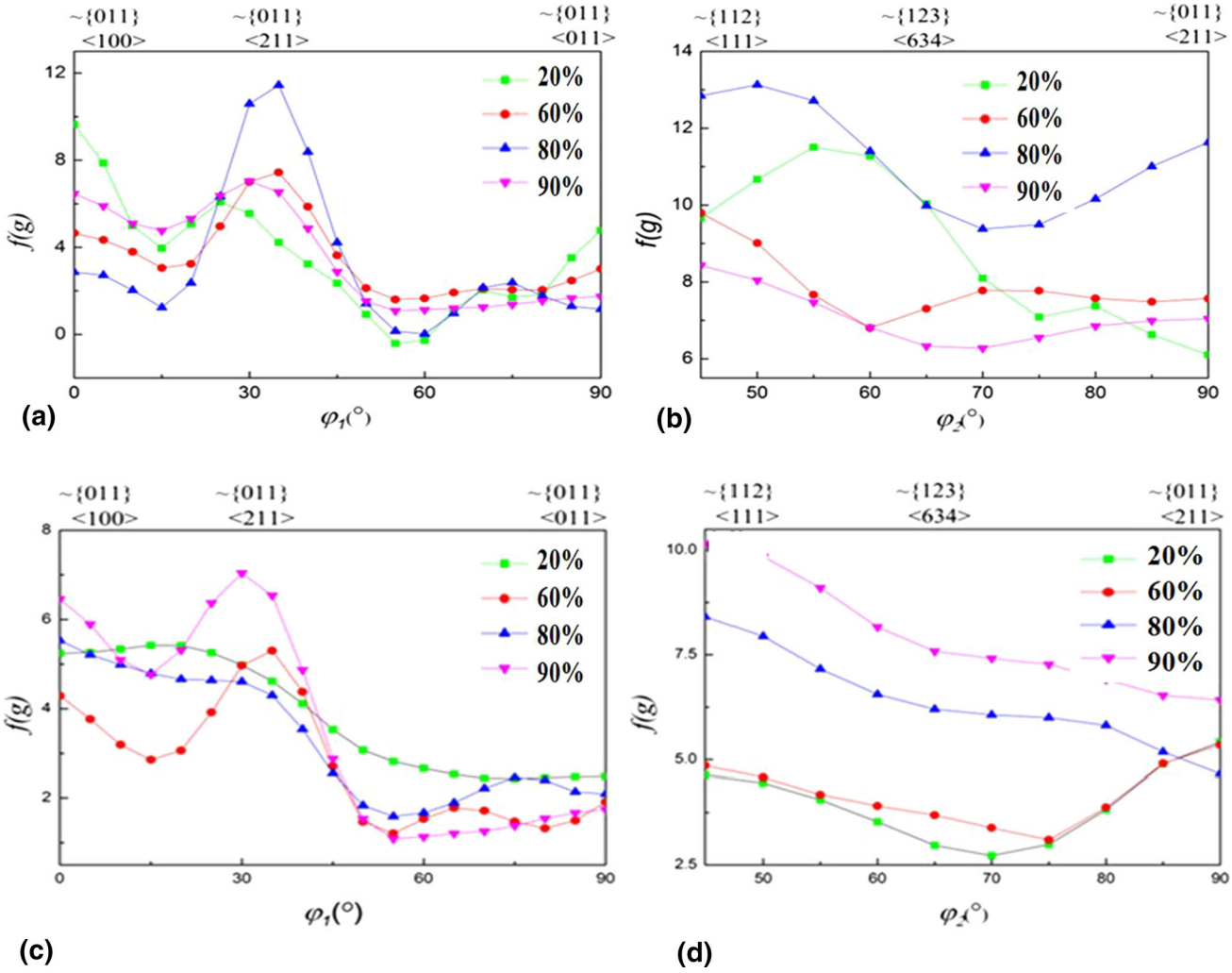

Fig. 3 The α-fiber (a, c) and β-fiber (b, d) of the RTR and CR sheet with different deformations

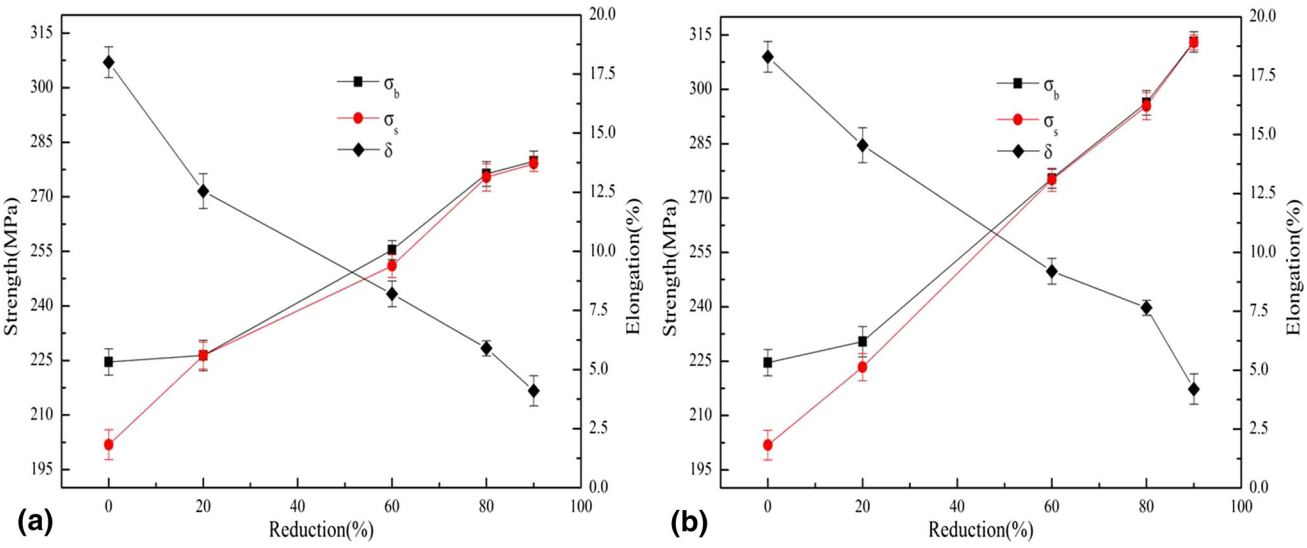

Fig. 4 The mechanical properties of the RTR (a) and CR (b) sheet with the different deformations

reduction. Thus, only ductile fracture occurred in the RTR sheet but ductile and intergranular fracture could be observed in the CR sheet after 20% rolling reduction. With increased degree of rolling, intergranular fracture became more obvious

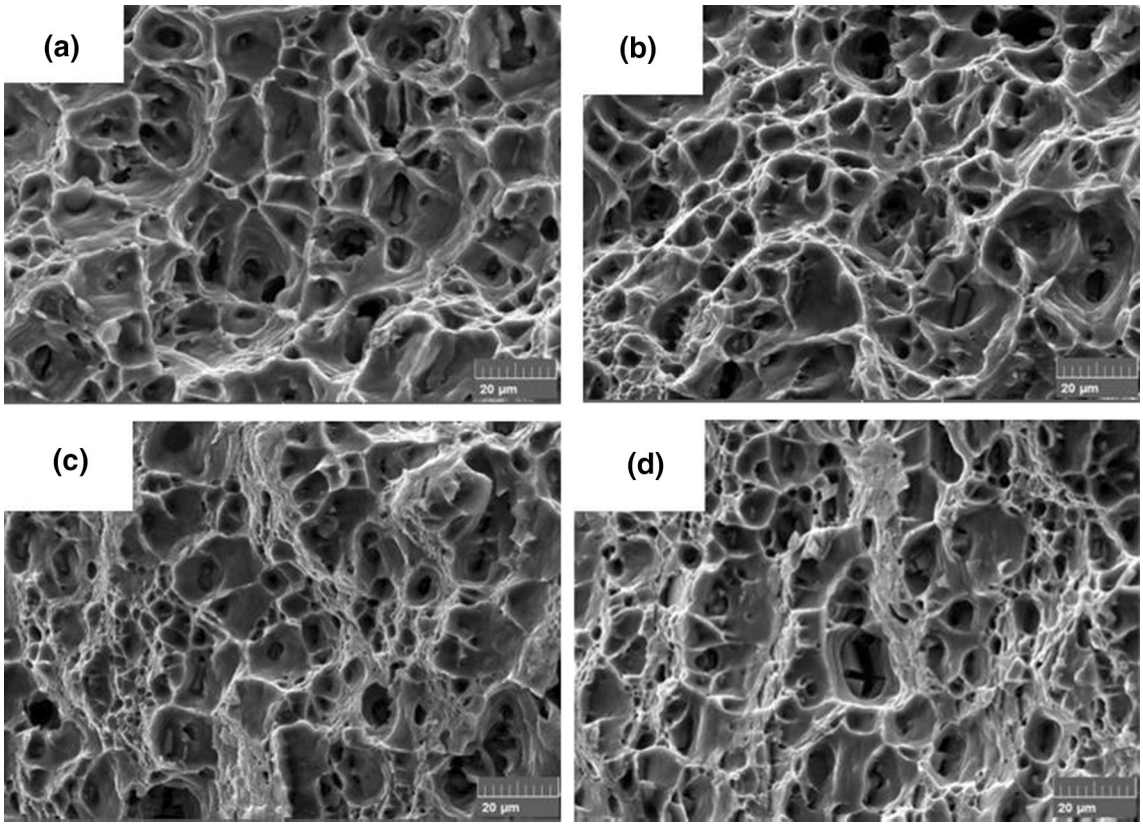

Fig. 5 The fracture morphology of the RTR sheet with the different deformation 20% (a), 60% (b), 80% (c), and 90% (d)

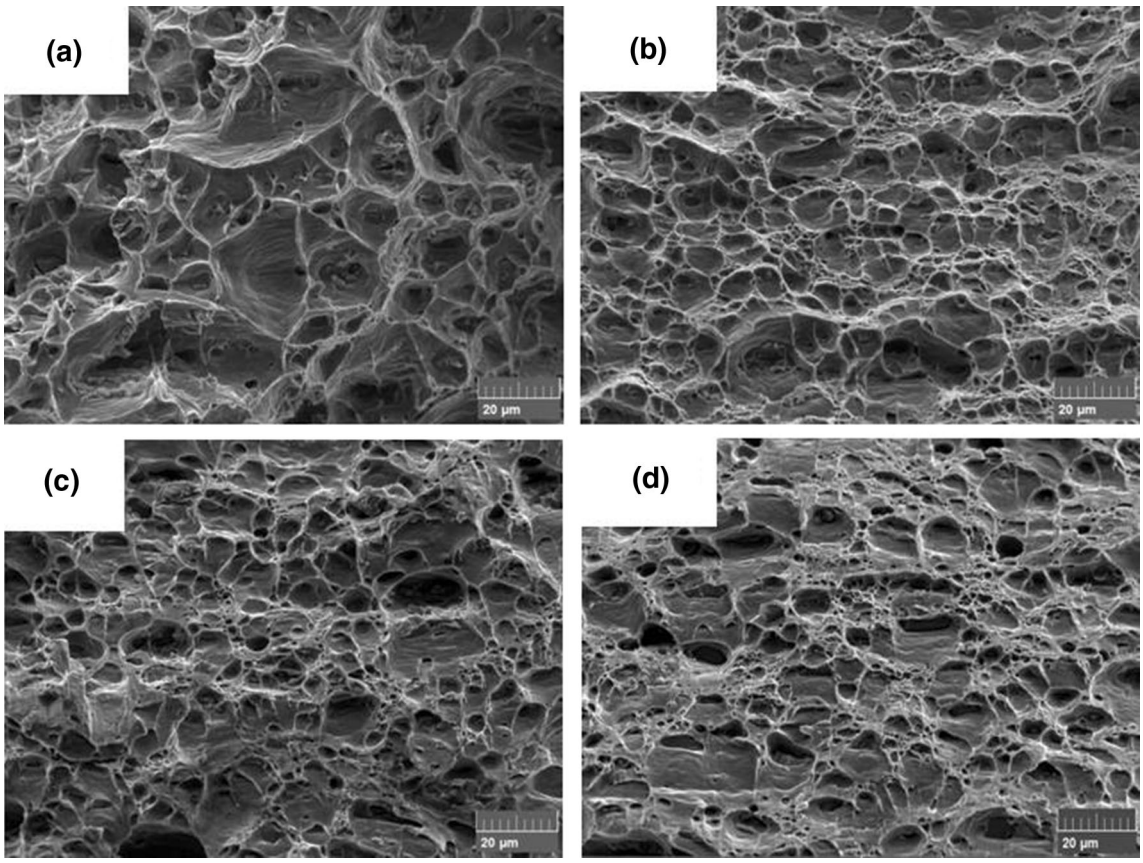

Fig. 6 The fracture morphology of the CR sheet with the different deformations 20% (a), 60% (b), 80% (c), and 90% (d)

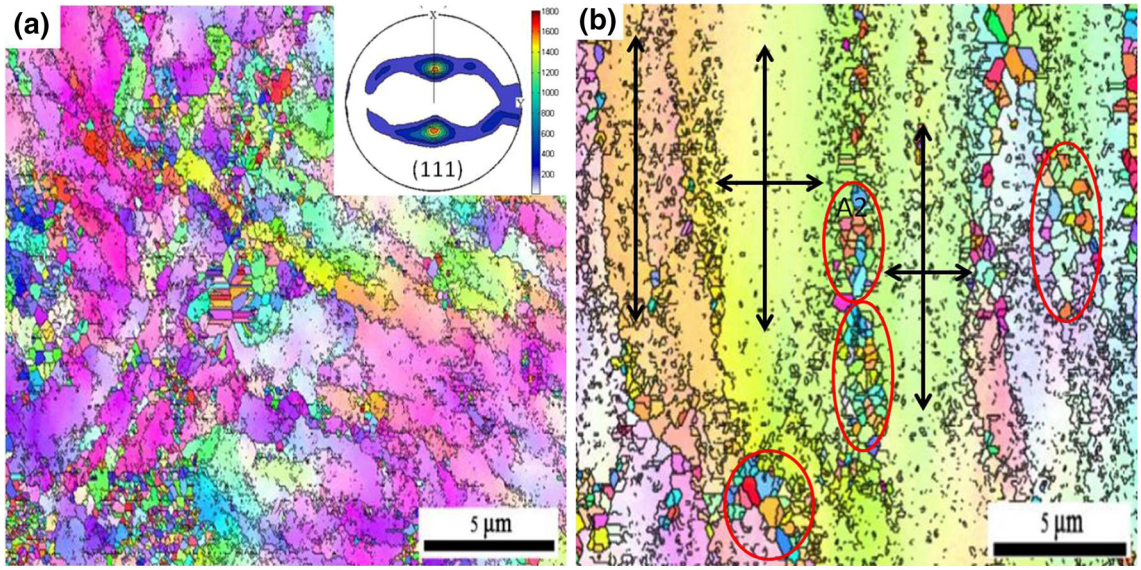

Fig. 7 The EBSD-micrographs of the 90% deformed sample. (a) CR sheet; (b) RTR sheet

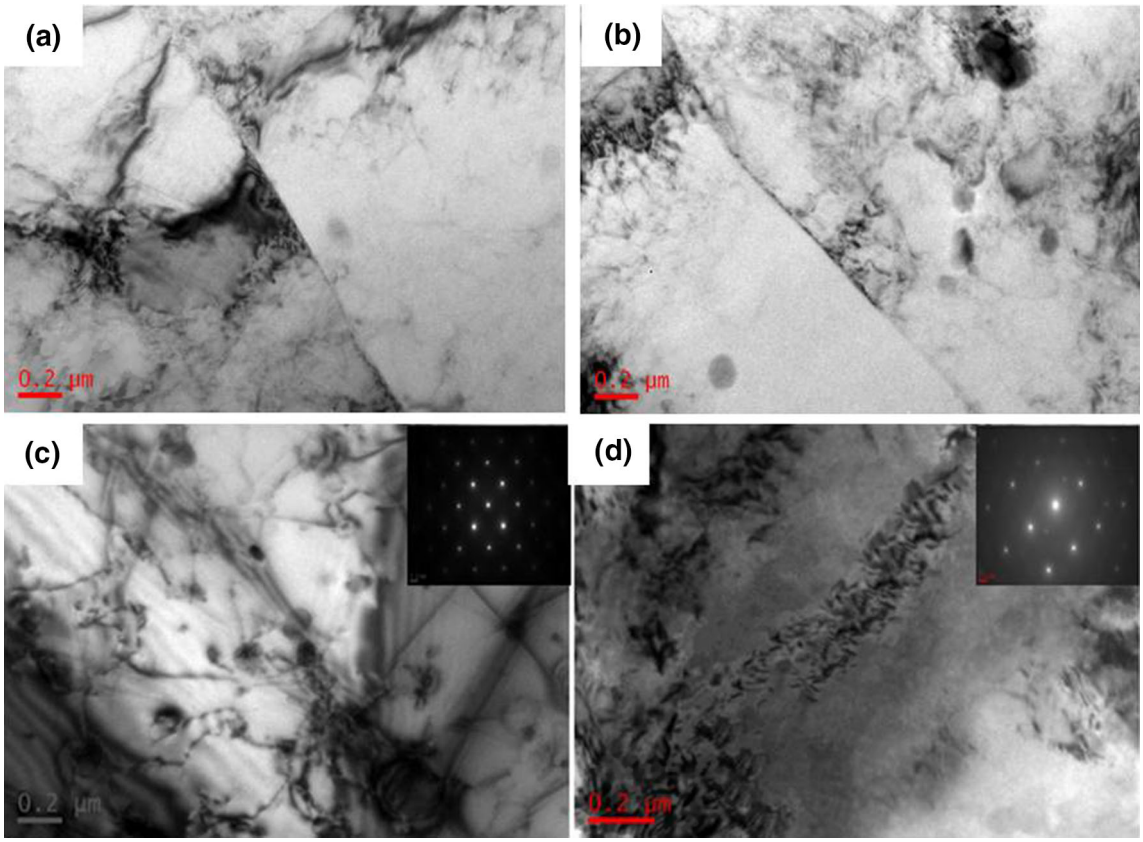

Fig. 8 The TEM-micrographs of the deformed sample. (a) CR sheet-80%; (b) RTR sheet-80%; (c) CR sheet-90%; (d) RTR sheet-90%

for the CR and RTR sheets. Furthermore, fracture of the ultrafine-grained structures caused the formation of small dimples. Because more energy was absorbed by the small dimples during the fracture process, the CR sheet exhibited higher strength than the RTR sheet, and similar results agreed with the literature (Ref 33).

5. Conclusions

1. Cryorolled suppressed the recovery and recrystallization of the rolled alloy sheet, preserving high dislocation density. A large number of ultrafine grains structures formed after 90% cryorolled.

2. Dislocations were impeded by the ultrafine-grained structure during deformation in the CR sheet. The strength of the CR sheet was improved through the combination of the ultrafine-grained structure and dislocation strengthening. The strength was improved by 10% and the plasticity was maintained for the CR sheet, as compared to the case of the RTR sheet.
3. Dimples and intergranular fracture were observed in the CR sheet during 20-90% rolling reduction. The strength was improved through the absorption of deformation energy by the fine dimples.

Acknowledgments

The project was supported by the program for the 973 Program (No. 2014CB046702). We are grateful M. A. Y. Li acknowledged.

References

1. Y. Aruga, M. Kozuka, Y. Takaki, and T. Sato, Effects of Natural Aging After Pre-aging on Clustering and Bake-Hardening Behavior in an Al-Mg-Si Alloy, *Scripta Mater.*, 2016, **116**, p 82–86
2. A. Serizawa, S. Hirosawa, and T. Sato, Three-Dimensional Atom Probe Characterization of Nanoclusters Responsible for Multistep Aging, *Metall. Mater. Trans. A*, 2008, **39**, p 243–251
3. V. Fallah, B. Langelier, and N. Ofori-Opoku, Cluster Evolution Mechanisms During Aging in Al-Mg-Si Alloys, *Acta Mater.*, 2016, **103**, p 290–300
4. M. Torsæter, H.S. Hasting, and W. Lefebvre, The Influence of Composition and Natural Aging on Clustering During Preaging in Al–Mg–Si Alloys, *J. Appl. Phys.*, 2010, **108**, p 3893–3896
5. G. Burger, A. Gupta, P. Jeffrey, and D. Lloyd, Microstructural Control of Aluminum Sheet Used in Automotive Applications, *Mater. Charact.*, 1995, **35**, p 23–39
6. X. Wang, M. Guo, Y. Zhang, H. Xing, Y. Li, J. Luo, J. Zhang, and L. Zhuang, The Dependence of Microstructure, Texture Evolution and Mechanical Properties of Al-Mg-Si-Cu Alloy Sheet on Final Cold Rolling Deformation, *J. Alloy. Compd.*, 2016, **657**, p 906–916
7. G. Dan Sathiaraj, P.P. Bhattacharjee, C.-W. Tsai, and J.-W. Yeh, Effect of Heavy Cryo-rolling on the Evolution of Microstructure and Texture During Annealing of Equiatomic CoCrFeMnNi high Entropy Alloy, *Intermetallics*, 2016, **69**, p 1–9
8. T. Bhattacharjee, I.S. Wani, S. Sheikh, I.T. Clark, and T. Okawa, Simultaneous Strength-Ductility Enhancement of a Nano-Lamellar AlCoCrFeNi 2.1 Eutectic High Entropy Alloy by Cryo-Rolling and Annealing, *Sci Rep*, 2018, **8**, p 3276
9. M. Yadollahpour, H. Hosseini-Toudeshky, and F. Karimzadeh, The Use of Response Surface Methodology in Cryrolling of Ultrafine Grained Al6061 to Improve the Mechanical Properties, *Proc. Inst. Mech. Eng. L J. Mater. Des. Appl.*, 2015, **230**, p 2
10. M. Yadollahpour, H. Hosseini-Toudeshky, and F. Karimzadeh, Effect of Cryorolling and Aging on Fatigue Behavior of Ultrafine-Grained Al6061, *J. Met.*, 2016, **68**, p 1446–1455
11. S.K. Panigrahi, D. Devanand, and R. Jayaganthan, A Comparative Study on Mechanical Properties of Ultrafine-Grained Al 6061 and Al 6063 Alloys Processed by Cryorolling, *Trans. Indian Inst. Met.*, 2008, **61**, p 159–163
12. H. Yu, L. Su, C. Lu, and K. Tieu, Enhanced Mechanical Properties of ARB-Processed Aluminum Alloy 6061 Sheets by Subsequent Asymmetric Cryorolling and Ageing, *Mater. Sci. Eng. A*, 2016, **674**, p 256
13. H.-L. Yu, A. KietTieu, C. Lua, and X.-H. Liu, Mechanical Properties of Al-Mg-Si Alloy Sheets Produced Using Asymmetric Cryorolling and Ageing Treatment, *Mater. Sci. Eng. A*, 2013, **568**, p 212
14. P. Nageswara Rao, D. Singh, and R. Jayaganthan, Effect of Post Cryorolling Treatments on Microstructural and Mechanical Behaviour of Ultrafine Grained Al-Mg-Si Alloy, *J. Mater. Sci. Technol.*, 2014, **30**, p 998–1005
15. Y.-C. Huang, X.-Y. Yan, and T. Qiu, Microstructure and Mechanical Properties of Cryo-rolled AA6061 Al Alloy, *Trans. Nonferrous Met. Soc. China*, 2016, **26**, p 12–18
16. Y.-C. Huang, X.-Y. Yan, Z.-B. Xiao, Z.-Y. Du, Y.-T. Huang, and T. Qiu, Texture Evolution and Fracture Mechanism of Cold Rolled AA6061 Alloy, *Mater. Sci. Eng. Powder Metall.*, 2015, **20**, p 585
17. T. Shanmugasundaram, B.S. Murty, and V. Subramanya Sarma, Development of Ultrafine Grained High Strength Al-Cu Alloy by Cryorolling, *Scripta Mater.*, 2006, **54**, p 2013–2016
18. V.L. Niranjani, K.C. Hari Kumar, and V. Subramanya Sarma, Development of High Strength Al–Mg–Si AA6061 Alloy Through Cold Rolling and Ageing, *Mater. Sci. Eng. A*, 2009, **515**, p 169–174
19. M. Murayama, Z. Horita, and K. Hono, Microstructure of Two-Phase Al-1.7 at% Cu Alloy Deformed by Equal-Channel Angular Pressing, *Acta Mater.*, 2001, **49**, p 21–29
20. K. Venkateswarlu, M. Chakraborty, and B.S. Murty, Influence of Thermo-Mechanical Processing of Al-5Ti-1B Master Alloy on its Grain Refining Efficiency, *Mater. Sci. Eng. A*, 2004, **364**, p 75–83
21. Y.C. Huang, Y. Liu, Q. Li, X. Liu, and C.G. Yang, Relevance Between Microstructure and Texture During Cold Rolling of AA3104 Aluminum Alloy, *J. Alloys Compd.*, 2016, **673**, p 383–389
22. F.J. Humphreys and M. Hatherly, *Recrystallization and Related Annealing Phenomena*, Pergamon, Oxford, 1996, p 16
23. O. Engler and K. Lucke, Mechanisms of Recrystallization Texture Formation in Aluminium Alloys, *Scr. Metall. Mater.*, 1992, **27**, p 1527–1532
24. R.Z. Valiev, R.K. Islamgliev, and I.V. Alexandrov, Bulk Nanostructured Materials from Severe Plastic Deformation, *Prog. Mater. Sci.*, 2000, **45**, p 103–189
25. Y. Huang and P.B. Prangnell, Continuous Frictional Angular Extrusion and Its Application in the Production of Ultrafine-Grained Sheet Metals, *Scripta Mater.*, 2007, **56**, p 333–336
26. A.P. Zhilyaev, G.V. Nurislamove, B.K. Kim, M.D. Baro, J.A. Szpunar, and T.G. Langdon, Experimental Parameters Influencing Grain Refinement and Microstructural Evolution During High-Pressure Torsion, *Acta Mater.*, 2003, **51**, p 753–765
27. P.P. Bhattacharjee and R.K. Ray, Effect of Processing Variables on Cube Texture Formation in Powder Metallurgically Prepared Ni and Ni-W Alloy Tapes for use as Substrates for Coated Conductor Applications, *Mater. Sci. Eng. A*, 2007, **459**, p 309–323
28. P.P. Bhattacharjee, M. Joshi, V.P. Chaudhary, and M. Zaid, The Effect of Starting Grain Size on the Evolution of Microstructure and Texture in Nickel During Processing by Cross-rolling, *Mater. Charact.*, 2013, **76**, p 21–27
29. P.P. Bhattacharjee, M. Joshi, V.P. Chaudhary, J.R. Gatti, and M. Zaid, Texture Evolution During Cross Rolling and Annealing of High-Purity Nickel, *Metall Mater Trans A*, 2013, **44**, p 2707–2716
30. J.R. Gatti and P.P. Bhattacharjee, Annealing Textures of Severely Cold and Warm-Rolled Al-2.5 wt% Mg Alloy, *J. Alloys Compd.*, 2014, **615**, p 950–961
31. N. Rangaraju, T. Raghuram, B.V. Krishna, K.P. Rao, and P. Venugopal, Effect of Cryo-Rolling and Annealing on Microstructure and Properties of Commercially Pure Aluminium, *Mater. Sci. Eng. A*, 2005, **398**, p 246–251
32. S.K. Panigrahi, K. Sushanta, and R. Jayaganthan, A Study on the Mechanical Properties of Cryorolled Al-Mg-Si Alloy, *Mater. Sci. Eng. A*, 2008, **480**, p 299–305
33. W.J. Kim and J.Y. Wang, Microstructure of the Post-ECAP Aging Processed 6061 Al Alloys, *Mater. Sci. Eng. A*, 2007, **464**, p 23–27